Study of reaction-diffusion controlled mass transport in stopped-flow fluidics for spatiotemporal multiplexing

Marcel Tintelott, Pradnya Gharpure, Yannick Coffinier, Xuan Thang Vu, Alexis Vlandas, Sven Ingebrandt, Vivek Pachauri

Study of Reaction-Diffusion controlled mass-transport in stopped-flow fluidics for spatiotemporal multiplexing

Marcel Tintelott[1§], Pradnya Gharpure[1§†], Yannick Coffinier[2], Xuan Thang Vu[1], Alexis Vlandas[2], Sven Ingebrandt[1], Vivek Pachauri[1*]

Affiliation(s):

1. Institute of Materials in Electrical Engineering 1, RWTH Aachen University, Sommerfeldstrasse 24, 52074 Aachen, Germany
2. IEMN, UMR 8520, Univ. Lille, CNRS, Univ. Polytechnique Hauts-de-France, 59000 Lille, France

Corresponding Author:

Dr. Vivek Pachauri; email: pachauri@iwe1.rwth-aachen.de; +492418027835

[§] These authors contributed equally

[†] Present address: Department of BioMechanical Engineering, Delft University of Technology, 2628 CD, Delft, The Netherlands

Keywords: Electrical biosensors, microfluidics, Lab-on-a-Chip, systems chemistry, molecular amplification

Abstract

Integration of biological reaction networks (BRNs) with biosensor platforms has emerged as a technological niche overcoming the challenges related to the loss of sensitivity and selectivity in biological media. Optimal operation of BRNs in microfluidics requires control over reaction-diffusion dominated mass-transport, heavily influenced by fluidic parameters. In this work, we study and design an on-chip platform combining a programmable unique molecular amplification (PUMA) as BRNs with nanoscale biologically sensitive field-effect transistor (BioFET) arrays, which employs a physical diffusion-barrier to gain spatial and temporal control over mass-transport. Computational and numerical approaches such as finite element (FEM) and finite volume methods (FVM) were implemented to solve partial differential equations numerically after domain approximation by numerous finite elements. The focus on geometrical optimizations of fluidics is aimed at mass-transport to occur with precise spatial and temporal control towards BioFET-arrays. Adopting a 0.5 pM limit-of-detection (LoD) for biochemical monitoring of BRNs via single-stranded deoxyribonucleic acid (ssDNA) output, we show that it was possible to compartmentalize the mass-transport spatiotemporally without cross-talk, which can be of critical advantage for using biosensor-arrays in order to realize a simplified multiplexed point-of-care biosensors.

1. Introduction:

Miniaturization of fluidics, in its various forms, continues to play a vital role in the study of reactions and mass transport in chemical and biological systems [1]. While fluidic circuits and use of low Reynold number flows have become a mainstream for the study of mixing and separation, study of reaction-diffusion phenomena in miniaturized stopped-flow fluidics only begins to see a resurgence of interest due to newfound applications in future technology [2, 3]. For example, regulation of biochemical/biomechanical conditions have high relevance for tissue engineering and development of Organ-on-a-Chip concepts for their dramatic influence on the vascularization and cell-growth [4-7]. The influence of three-dimensional (3D) geometry and various other physical parameters on the mass-transport of metabolites and biomolecules has been studied recently in various cell-lines, giving way to self-organization, differentiation patterns and novel approaches in developmental biology with precision biofabrication [4, 8-10]. Beyond such topics related to self-organization of cells and tissues, spatiotemporal control of mass transport at nanoscale is also proving to be helpful in the study of various biomolecular systems of cell such as lipid and protein structure of cell membrane, gene-expression networks in relation to cellular heterogeneities and development of next generation microfluidics for dynamic single-cell spatial and multimodal transcriptomic [11, 12].

Even before, spatiotemporal distribution of chemical species had received attention for the study of non-equilibrium reactions [13-18]. A famous example of such a non-equilibrium systems that has continuously attracted scientific attention is the Belousov-Zhaboutinskii (BZ) reaction as a type of chemical oscillations and self-organization in chemical waves[19]. Ever since, temporal and spatial variation of reaction constituents and products of such non-equilibrium reactions in homogeneous conditions has been a topic of great interest, as a simplified model of self-organization in complex biochemical and biological systems [20]. More recently, study of such out of equilibrium systems in miniaturized fluidics helps mimicking complex systems such as biochemical reaction networks (BRNs), biochemical oscillators (BOs), self-assembly and molecular motion and advancing our understanding of systems chemistry [2, 16, 21-25]. At the same time, scientific interest in the study of heterogeneous non-equilibrium reactions began with the discovery of oscillatory kinetics at interfaces. A well-studied example of such heterogeneous reaction system is the catalytic oxidation of carbon monoxide (CO) at Pt(110) surface, also catalysing the development of experimental methods such as scanning photoelectron microscopy and photoemission electron microscopy for the imaging such systems with high temporal and spatial resolutions [17]. Eventually, development of theoretical models for the heterogeneous oscillatory reactions elucidating the underlying microscopic mechanism gave a significant boost for the study of such systems at the solid-liquid interface where reaction-diffusion patterns of reaction constituents play a pivotal role in self-organization [18].

Interestingly, the reaction-diffusion regulated spatiotemporal mass transport has a direct relevance for technologies such as nanopores, miniaturized point-of-care (PoC) biosensors and micro-reactors for

biological and chemical processes [26-28]. On-chip biosensors based on nanoscale transducers such as semiconductor nanowires (s-NWs), microelectrode arrays (MEAs) and two-dimensional (2D) materials where biological interactions take place at the solid-liquid interface, are suitable examples where stopped-flow fluidics provide an easy solution for sample handling and are prone to influences from diffusion related aspects [29-32]. Such biosensor platforms typically employ volumes in the range of tens of microliters and generate different mass-transport regimes based on the molecular concentrations in the bulk and on the surfaces, density of the medium, retention time and the shape of the fluidic volumes [33, 34]. At the same time, new strategies of integrating BRNs in microfluidics for molecular recognition and programmable unique molecular amplification (PUMA) are getting popular for advantages such as enhanced selectivity and reliable transduction [35, 36]. Similar to the well-known polymer chain reaction (PCR) technique the PUMA can be used to amplify nucleic acid sequences. In contrast to the PCR technique, the PUMA utilizes isothermal conditions for the amplification of nucleic acid sequences. The molecular reaction mixture consists of multiple DNA templates and an enzyme mixture for the amplification. The onset of the amplification cascade is depending on the input concentration of the targeted nucleic acid sequence (e.g. miRNA). Therefore, the amplification onset as a function of time can be used to determine the input concentration of the targeted nucleic acid sequence. A detailed step by step description of the mechanisms behind the PUMA reaction is provided in the supplementary materials. Such BRNs, after modifying their recognition template sequence, are also able to provide modular mechanisms for multiplexed detection of low-concentration biomarkers such as microRNAs and signalling proteins [36, 37]. Here, optimal operation of BRNs requires study of 3D mass-transport profiles in stopped-flow fluidics on chip at moderately higher temperatures.

Biologically sensitive ion-sensitive field-effect transistors arrays (Bio-FET arrays) are classified as highly sensitive biological transducers for biomedical applications [38]. The possibility of micromachined fabrication ensures a low-cost production of such sensors. However, one of the most prominent bottlenecks of such near-field charge sensitive devices is the highly decreasing sensitivity in biological relevant analytes. Such liquids contain a high amount of salts which results in a lowering of the Debye-screening length – one of the most critical parameters in near-field charge detection – and, thus, results in a drastically decrease in sensitivity of the biosensor. Therefore, an on-chip amplification of the targeted nucleic acid sequence is of high interest to overcome this fundamental limitation, which was demonstrated in the literature [39, 40]. However, when it comes to miRNA profiling, a multiplexed readout scheme is mandatory to determine the health condition of a patient. For instance, the miRNA Let-7a level expression is affected by multiple types of cancer (e.g. breast, lung, or prostate) [41]. Therefore, multiple miRNA target sequences need to be detected simultaneously. To tackle the need for on-chip amplification in combination with a multiplexed readout, we performed numerical simulations as described in the following.

A BioFET-arrays platform based on Si NWs, dedicated for the integration of PUMAs for biodetection can be seen in **figure 1**. The simulation design is based on recently published biosensor platform from our group combining a Si NW array with on-chip temperature sensors and metal or graphene oxide/polymer hybrid reference electrodes [42, 43]. The platform includes a 4 mm wide stopped-flow fluidic chamber placed on top of biosensor chip having an array of BioFETs, arranged in a straight line. Different PUMA-BRNs unique to micro ribonucleic acid (miRNA) biomarkers are surface immobilized on the distal ends of the fluidic ceiling, from where they release a common ssDNA sequence, upon recognition of desired miRNA. The PUMAs can be modified such that they recognize different microRNA sequences and cascade this molecular recognition to production of a common short DNA sequences. Programming PUMAs as such allows BioFETs having the same receptor-DNAs for the electrical detection of ssDNA and thereby simplifying the assembly of the biosensor chips for real applications. Therefore, stopped-flow conditions are required to ensure a spatiotemporal multiplexed readout using a common ssDNA output for multiple PUMA networks. Stopped-flow conditions ensure that diffusion is the prominent mode of mass transfer in the fluidic system, and hence, the transport of the PUMAs to the biofunctionalized surface is governed by the concentration gradients developed. Further, to ensure multiplexing capabilities of the proposed sensor system a local starting point of the diffusion front is needed to detect the spatiotemporal spread of the diffusion wave. This can be realized by immobilizing the recognition template of the PUMA at both sides of the fluidic channel (e.g. at the top glass cover). Without an external triggered flow, the generated nucleic acid sequences would diffuse though the channel with a uniform velocity and bind to the surface of the BioFET arrays [44]. Due to the binding of the generated ssDNA sequences a change in the surface potential of the BioFET would result in a change in the current flow. Stopped-flow conditions are realized when no external pressure gradient is applied. Therefore, the mass-transport inside the fluidic volume only consists of diffusion. In this work, we present numerical investigations of the reaction-diffusion regulated mass transport of ssDNA inside such a complex microfluidic volume operating BRNs in biological conditions and study the impact of fluidics shape on spatiotemporal multiplexing. We show that geometrical optimizations of the fluidic volumes by implementation of simple diffusion barriers significantly retard the mass-transport process. Thus, with simple barrier geometries too, the mass transport can be controlled and retarded to prevent cross-talk in scenarios where multiple different ssDNAs are to be detected. Further, we show that by changing the shape of such diffusion barriers, it is possible to tune the reaction-diffusion profiles (wave fronts) and set specific periods for the onset of hybridization process at the BioFET-arrays.

2. Materials and Methods

2.1. The reaction-diffusion system:

Diffusion as a mass transport phenomenon involves an entity of interest (e.g. biomolecules) moving from a point of higher concentration (or higher pressure) to that of a lower concentration (or lower pressure) in a given medium, thereby forming a concentration gradient. When the concentrations are also dependent on the rate and/or order of a chemical reaction involved (the diffusing species also participates in a chemical reaction), the system is called a reaction-diffusion system. Typical examples of such systems are chemical reaction-diffusion networks such as BZ reactions and autocatalytic BRNs such as PEN-DNA and PUMA molecular programs [36, 45, 46]. Such systems, governed by diffusion equation, can be mathematically described by the Kolmogorov-Petrovskii-Piscuno (KPP) equation [47]. The KPP equation describing the reaction-diffusion front in a fluidic volume is defined as

$$\frac{\partial c}{\partial t} = D\frac{\partial^2 c}{\partial t^2} + R(c) \quad \text{.....(1)}$$

- where, c denotes the molecular concentration as a function of space and time c(x, t), D is the diffusion coefficient of candidate biomolecules with concentration c, and R represents the local reaction term that describes the reaction rate and order. In the absence of convection and bulk fluid motion, equation 1 does not include the term for the velocity field of the fluid. Such a formulation also assumes isotropic diffusion conditions where D does not depend on the location in the fluidic volume.

2.2. Molecules under spatial reaction-diffusion:

The autocatalytic PUMA-BRN considered for this work were designed for the detecting the presence of miRNAs that are specific biomarkers for neurodegeneration disorders [37, 48]. Briefly, PUMA employs an exponential molecular amplification cascade after the recognition of a miRNA target sequence at the converter template, which results in the synthesis of 12bp ssDNA. As this autocatalytic BRN is maintained by the use of ligase, nickase and polymerase enzymes, a buffer medium and elevated temperature of 45 - 50 ^{0}C is required in the fluidic volume to ensure enzymatic activity. When the PUMA starts at a certain position in a microfluidic channel such as shown in the figure 1b, the trigger will create a reaction-diffusion front, which are expected to propagate along the fluidic volume. The maximum PUMA output (12bp ssDNA) was assumed to be at a concentration of 1 µM, and thus the maximum capacity of the system too was considered to be 1 µM.

2.3. Fluidic Simulation Framework:

A computational model of stopped-flow fluidic volume under study (4 mm length, 50 µm width, and 800 µm height) was developed to simulate the diffusion mass transport and the reaction dynamics. Computational and numerical techniques such as Finite Element Method and Finite Volume Method were applied to solve the complex partial differential equations and domain approximation by numerous finite elements. The 2D and 3D design of fluidic volumes were carried out in SOLIDWORKS™ and imported to the COMSOL™ Multiphysics™ interface. The modules used for simulations of diffusive mass-transport in

COMSOL™ Multiphysics comprised of the 'Transport of Diluted Species' and 'Reaction Engineering' which accounted for the diffusion and the reaction rates, both from equation 1. The reactive term was used to couple the two modules and model the complete system.

The system modelled in the work is governed by reaction-diffusion physics. The mass transfer occurs through diffusion, the system being of stopped-flow nature, and the convection being absent. Further, the concentration gradient that drives the mass transfer by diffusion is also impacted by the autocatalytic reaction of the PUMAs, making it a reaction-diffusion system. Simulation of time domain variation in the diffusion profile was monitored for a constant supply of 1 μM DNA from the release spots 1 and 2 (figure 1). DNA concentration in the fluidic volume shall then vary with time based on KPP form of the Partial differential equation for reaction-diffusion and this variation was studied. To reduce the complexity of the simulations the reactions of the molecular program products with the biofunctionalized surface (surface reaction kinetics at the Si NW interface) were neglected. Only the diffusion profile of the trigger was investigated, after initiation of the autocatalytic reaction-diffusion front from the inlet positions as shown in Fig 1

In order to retard or restrict the diffusion of certain species in a reaction-diffusion system thin films have been studied and applied as a diffusion barrier in many instances [49]. Taking the concept of diffusive mass transfer in the microchamber further, the work intended to model such a diffusion barrier concept and study the impact of the same on the diffusion profile in the microfluidic chamber. The geometries of a possible barrier, based on feasibility from a fabrication point of view were modelled and investigated (figures 3, 4 and 5). These structures can be easily fabricated using additive manufacturing processes like stereolithography, fused filament fabrication and standard polydimethylsiloxane processes.

The temperature was set to 50°C that suits the functioning of the PUMA-BRNs. The reaction rate constants and carrying capacities were set as global variables, and the domain properties were assigned along with concentration and no flux boundary conditions. As the model pertained to a stopped-flow system with no bulk flow, convection effects were not taken into account in these simulations. The medium of diffusion was set to a buffer with a 150 mM initial concentration, and the DNA strand diffusion coefficient was estimated from empirical relations from literature for a 12-base pair DNA [50]. The rate expression applied based on the Fisher KPP form of the reaction-diffusion system was:

$$R = K_f A(1 - \frac{A}{C})$$

……..(2)

where, K_f is the forward rate constant, A is the concentration of species, and C is the maximum nucleic acid carrying capacity of the system (in other words: the maximum generated amount of the ssDNA output of the PUMA reaction system). To perform the simulations we assumed a carrying capacity of 1 μM, which

creates the constant output of the PUMA. Here, we only considered the forward rate constant K_f since the reverse reaction constant K_r can be neglected for specific target receptor combinations [50].

3. Results and Discussion

3.1. ssDNA mass-transport in the fluidic volume:

According to the Fisher KPP rate law and reaction kinetics parameters for a DNA autocatalytic replication in BRN, the diffusion was simulated in a time dependent 3D model for up to about 2 hours (>120 minutes) [44]. Implementing the simulation of reaction-diffusion of single species (12bp DNA with 1μM conc.) at the release spot (surface functionalized PUMA), a time dependent diffusion profile for the given fluidic volume is shown in the figure 3. In order to speed up the simulation, a two-dimensional vertical profile simulation was carried out to study the vertical spread of diffusion front produced by PUMA-BRNs. As shown in figure 3 the diffusion front spread out along the whole channel within 36 minutes. Assuming that the bottom part of the channel contains an array of receptor-DNA modified BioFETs, the spatiotemporal diffusion could be monitored in real-time.

3.2 ssDNA mass-transport with a diffusion barrier:

As mentioned earlier, in order to retard the diffusion of PUMA-BRN output (12 bp DNA), introduction of diffusion barrier and simulation of mass transport was attempted. Several geometric iterations were carried out to find an optimal geometry of such a diffusion barrier. On the introduction of a diffusion barrier, the simulation domain was divided geometrically, and distinct properties were assigned to each part. The barrier itself was assigned transport properties such that the diffusion through it would be absent. At first, the barrier was conceptualised as a cube, and then geometric changes to engineer the mass-transport in the fluidic volume were evaluated as follows:

a. *Cuboid Diffusion Barrier*: As shown in the illustration in figure 3a, a cuboid diffusion-barrier with dimensions of 1 mm length and 0.78 mm depth was placed under the ceiling of the fluidic volume, virtually partitioning it while leaving a fluidic capillary with 1 mm length, 50 μm in width and a height of 20 μm. The graphs 3b-3e as shown in figure 3 depict of the resulting diffusion patterns when DNA is injected from the left inlet (PUMA1) and observed in the form of a 2D simulations evaluating the effect of the barrier in comparison to fluidic volume with no barrier (figure 2). The barrier is found to be effective in preventing fast diffusion throughout the microfluidic volume for up to 30 to 50 minutes. With more time elapsed, however, the build-up of DNA concentration across the diffusion barrier progresses very fast, which is undesirable. With PUMA-BRNs amplification profiles typically longer than 50 minutes, this quick build-up of the DNA output after 50 minutes would result in significant molecular cross-talk between PUMA1 and PUMA2 BRNs, and therefore calls for optimization of barrier's geometry.

b. Trapezoid Diffusion Barrier, Type 1: In order to minimize the molecular cross-talk between different BRNs in the same fluidic volume, a trapezoidal diffusion barrier was studied as an alternate geometry. This configuration is shown in the figure 4a where the trapezoid barrier is placed in between and has 1 mm length at the base and 50 μm width. The depth of the barrier is selected as 790 μm leaving a gap of 10 micron to the BioFET chip underneath. This way the fluidic capillary has an effective dimension of 1.6 mm (length), 50 μm (width) and 10 μm (height). The simulations were carried out in a similar way and the mass transport profiles are shown in the figures 4 images b-e from the beginning up to 44, 69 and 125 minutes. Here, the speed of the reaction-diffusion front along the diffusion channel was retarded in the comparison to the cuboid barrier. After about 120 minutes, the total DNA concentration, on the other side of the diffusion barrier, was reduced to approximately 0.5 μM.

b. Trapezoid Diffusion Barrier, Type 2: In the final iteration, the height of the diffusion channel was further reduced to 5 μm while keeping the overall trapezoidal shape of the barrier. The overall configuration is shown in figure 5. From the reaction-diffusion profiles as shown in figure 5b-e, at 0, 55, 100 and 120 minutes respectively, the speed of the diffusion front is clearly reduced, and a reduced DNA concentration (0.3 μM) was reached after 120 minutes. The height of the diffusion channel, therefore, has a significant impact on the mass transfer along the diffusion channel. Overall, this configuration enabled an efficient retardation of the diffusion process for 12bp DNA optimal for the implementation of several BRNs on same chip.

3.3. Spatiotemporal control and multiplexed read-out:

In order to simulate spatiotemporal multiplexing using such a reaction-diffusion regulated fluidics system, two different DNA sequences were modelled to be continuously injected from the two release spots 1 and 2 respectively as shown in the figure 6. Upon applying of identical physical properties e.g. diffusion coefficient and reaction rate expressions for each of them, the diffusion patterns were symmetrical depicting the qualitative accuracy of the model. To be more application specific, especially in case of biosensors where a spatiotemporal multiplexing is advantageous to create more versatile and adaptive sensor chip platforms, we considered the release spots 1 and 2 as the PUMA, which upon the presence of a target biomarker, trigger an enzymatically controlled exponential amplification reaction (EXPAR) providing an exponential supply of short DNA sequences as an output for a limited time. This EXPAR typically lasts for a few hours, saturates, and then decays exponentially. The PUMA can be surface immobilized as shown in this scheme and modified by changing the converter DNA template to recognize a specific biomarker such as miRNA. In our case, PUMA were optimized to give an exponential onset (readable by rtPCR) against 0.5 pM concentration analyte biomarker (miRNA) within 5 minutes and then saturation point occurring around half an hour. Given when reaction-diffusion regulated microfluidic volume is spatially engineered in order to distinguish the mass-transport from *n* number of release spots, with the help of nanowire arrays, modular sensor platforms can be developed. Such a modular sensor platform alleviates the requirement of surface

modifying the sensor-spots with different receptor/probe DNA sequences using complicated procedures. Ideally, tuning of the PUMA at release spots would allow a biomarker linked mass-transport that is detected by the sensors in an engineered time-domain. For example, higher concentration of a biomarker would lead to an earlier onset of PUMA and requires slowing down of the reaction-diffusion driven mass transport. Here, we applied our simulation framework to evaluate the PUMA output sequence concentrations at a specified sensor position (BioFET-array) on the chip (figure 6). In order to do this, a transverse sectional profile was drawn in the simulation model in order to extract the concentration data at the BioFETs interface closest to PUMA1 (figure 6b). The build-up of the output DNA concentration at a single BioFET located near the release spot 1 are shown in the graph (figure 6a). In this case, primary sensor requirements are to prevent a non-specific interaction due to a crosstalk (i.e. between the trigger from spot 2 and spot 1) to ensure that correct PUMA-specific output is encoded by the BioFETs. It was considered that the BioFETs are able to encode the DNA output concentrations greater than 0.5 pM set as the limit of detection (LoD). This LoD is represented by the horizontal line in the graph. Then the simulations evaluate the local DNA concentrations at the BioFET originating from PUMA1 and PUMA2, respectively. While the blue curve shows concentration profile evolution at the BioFET interface as a result of reaction-diffusion mass-transport from PUMA2, the red curves show evolution of concentration profiles at the BioFET interface when PUMA1 starting at the same time as PUMA2, i.e. 0 minutes delay. A comparison of these 2 curves demonstrates that up to 80 minutes, the BioFETs will detect the output from PUMA1 exclusively without any interference from PUMA2 due to slowing down of the mass-transport across the diffusion barrier. The yellow, purple and green curves also evaluate a situation, when the PUMA1 starts with a certain time delay given as 6, 35 and 60 minutes, respectively. The evaluation suggests that a delay of up to 60 minutes (typical amplification time) can be easily set-up between the onset of two PUMAs and exclusive detection of the output DNA sequences from PUMA1 or PUMA2 in a spatiotemporal manner (26). We intend to adopt such engineered fluidic volumes with our BioFET-array chips in order to virtually compartmentalize the molecular output from different PUMAs surface immobilized onto the ceiling of fluidic layer and carry out spatiotemporal detection of different biomarkers. In addition, spatiotemporal engineering of mass-transport on chip is expected to facilitate study of more complex programmable molecular cascades and help setting up robust platform for studies of molecular biocommunication strategies using nanoelectronics. Additional data for the time-dependent ssDNA propagation within the microfluidic channel can be found in the supplementary materials.

4. Conclusion:

In this work, we studied the mass-transport of small DNA sequences (12bp) as an output of programmable unique molecular amplification (PUMA) systems spatially arranged in a stopped-flow fluidic volumes. With an aim towards integration of a biosensor platform for multiplexed detection, biomarker-specific PUMAs

were considered, and a reaction-diffusion approach was adopted to simulate the evolution of DNA concentrations at BioFET-arrays at the bottom of the fluidic volume. For effective spatiotemporal multiplexing, it was required to engineer the mass-transport in the given fluidic volume by using physical barriers and optimize build-up of output DNA concentrations related to different PUMAs, for a mutually exclusive electrical detection by BioFETs. For this, septa with different shapes and sizes were considered tuning the reaction-diffusion controlled mass-transport. We demonstrate that use of such septa has a critical influence on the mass transport and can lead to an enormous retarded diffusion along the diffusion channel. We show that the cuboid septum resulted in a final DNA concentration of around 0.8 µM after 120 minutes, while an optimized diffusion channel reduced the amount of DNA to approximately 0.3 µM. The geometry of the diffusion channel determines the diffusion speed of the reaction-diffusion front along the channel. Firstly, we show that the length of the diffusion channel should be as high as possible to increase the diffusion length and thus slowing down the speed of the reaction-diffusion front. Secondly, the height of the diffusion channel should be minimized to further reduce the diffusion speed. Finally, we evaluate that in such a fluidic volume engineered for optimal operation of PUMAs, a delay of up to 60 minutes between the start of two molecular programs does not lead to any significant biochemical cross talk. It is expected that integration of spatiotemporal fluidics with PUMA powered biosensors will allow modular strategies for multiplexed detection in near future. Overall, spatiotemporal control over mass-transport in confined volumes like attempted in this work also opens up possibilities to realize on-chip platforms to implement and study complex BRNs, as a topic of fundamental interest in self-organized systems.

5. Supplementary Material

The PUMAs considered for the spatiotemporal multiplexing and further details on mass-transport profiles with and without the use of different kinds of diffusion barriers are discussed in the supplementary material. Link:

6. Acknowledgments

The authors thank the German Research Foundation (DFG) for funding the research project “Molecular Programs for neurodegenerative diseases markers Biosensing” (Project no. 391107823).

FIGURES

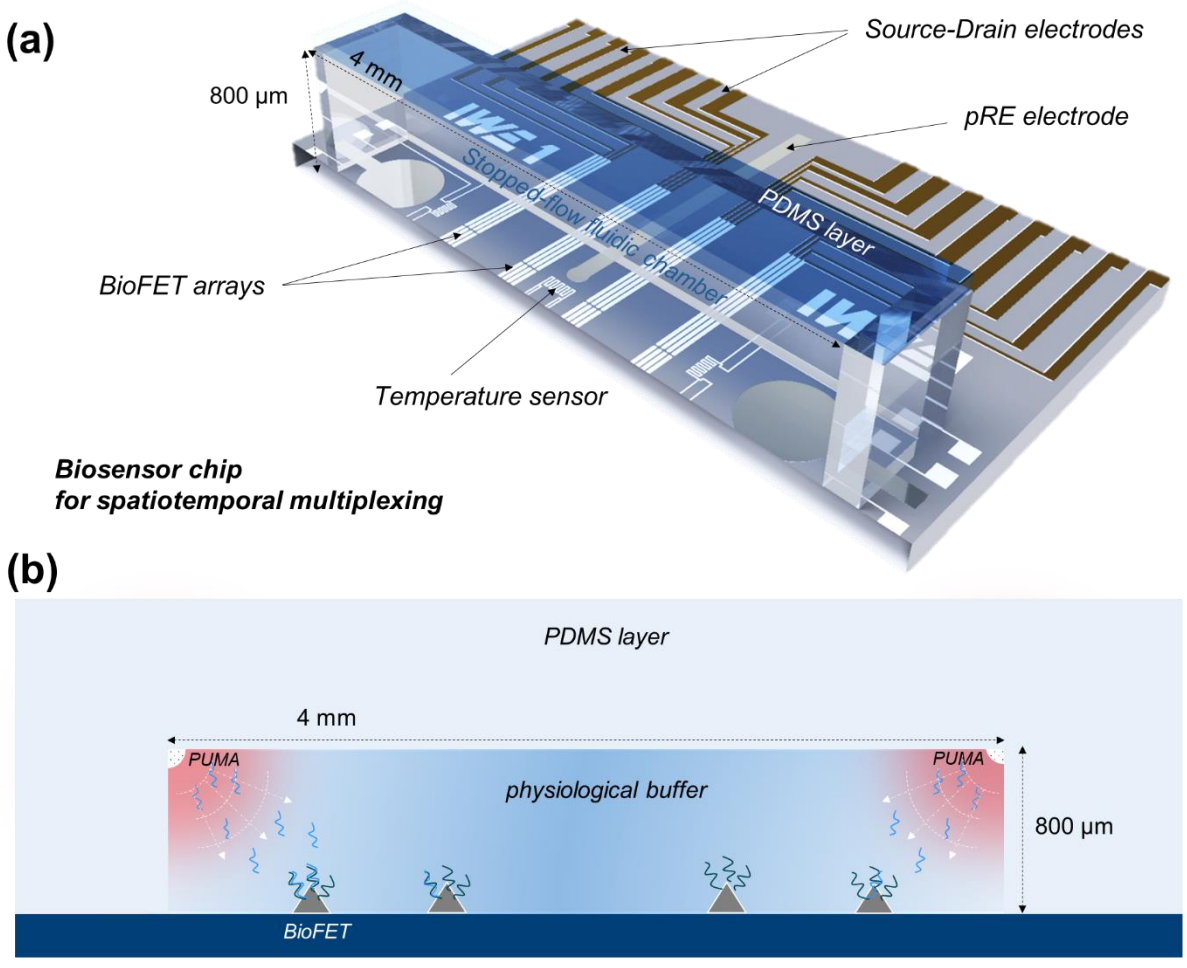

Figure 1: Schematic illustration of the biosensor platform modelled for spatiotemporal multiplexing with the help of programmable ultrasensitive molecular amplification (PUMA) reactions and stopped-flow fluidic chamber aimed at reaction-diffusion controlled mass transport. (a) Our biosensor chip with biologically sensitive ion-sensitive field-effect transistors arrays (BioFET-arrays) dedicated for running such PUMA in small fluidic volumes at elevated temperatures is shown with the fluidic layer on top. (b) A vertical cross-section of the biosensor platform shows the fluidic volume filled with the physiological buffer and the PUMA surface functionalised on the fluidic layer's ceiling towards left and right extremities. In the presence of the analyte (trigger for PUMA), an amplification reaction starts with exponential onset of short output DNA (12bp) sequences which are diffusing into the fluidic volume of dimensions 4 mm × 800 µm × 50 µm ($l \times h \times w$). Optimal engineering of the spatiotemporal concentration profile of the output DNA sequences and programming of PUMA for different analyte biomarkers facilitates biosensor multiplexing where different BioFETs specifically sensitive to the PUMA output DNA provide an ultrafast measurement of local concentration at the interface (bottom of the fluidic chamber).

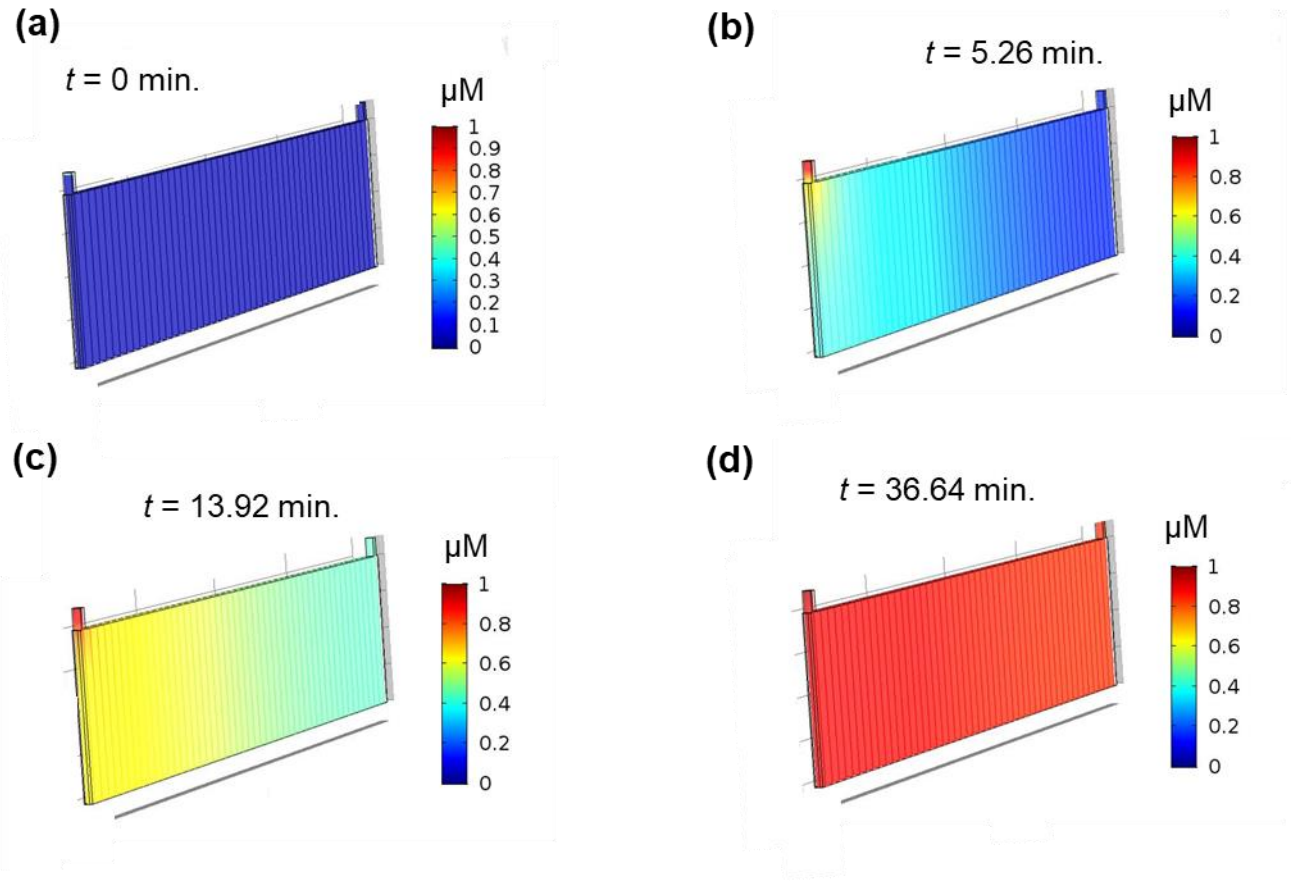

Figure 2: Three-dimensional spatiotemporal mapping of the reaction-diffusion dominated mass transport in stopped-flow fluidics integrated on top of biosensor chip. (a) In the beginning (t = 0 min), the fluidic volume is filled with the background electrolyte (physiological buffer) and is devoid of any biomolecule under study (12bp ssDNA). (b) ssDNA being introduced at the virtual inlet with a concentration of 1 μM. ()Reaction-diffusion profiles at different time stamps: (top left) 0 minutes, (top right) 5.3 minutes, (bottom left) 13.9 minutes, (bottom right) 36.6 minutes.

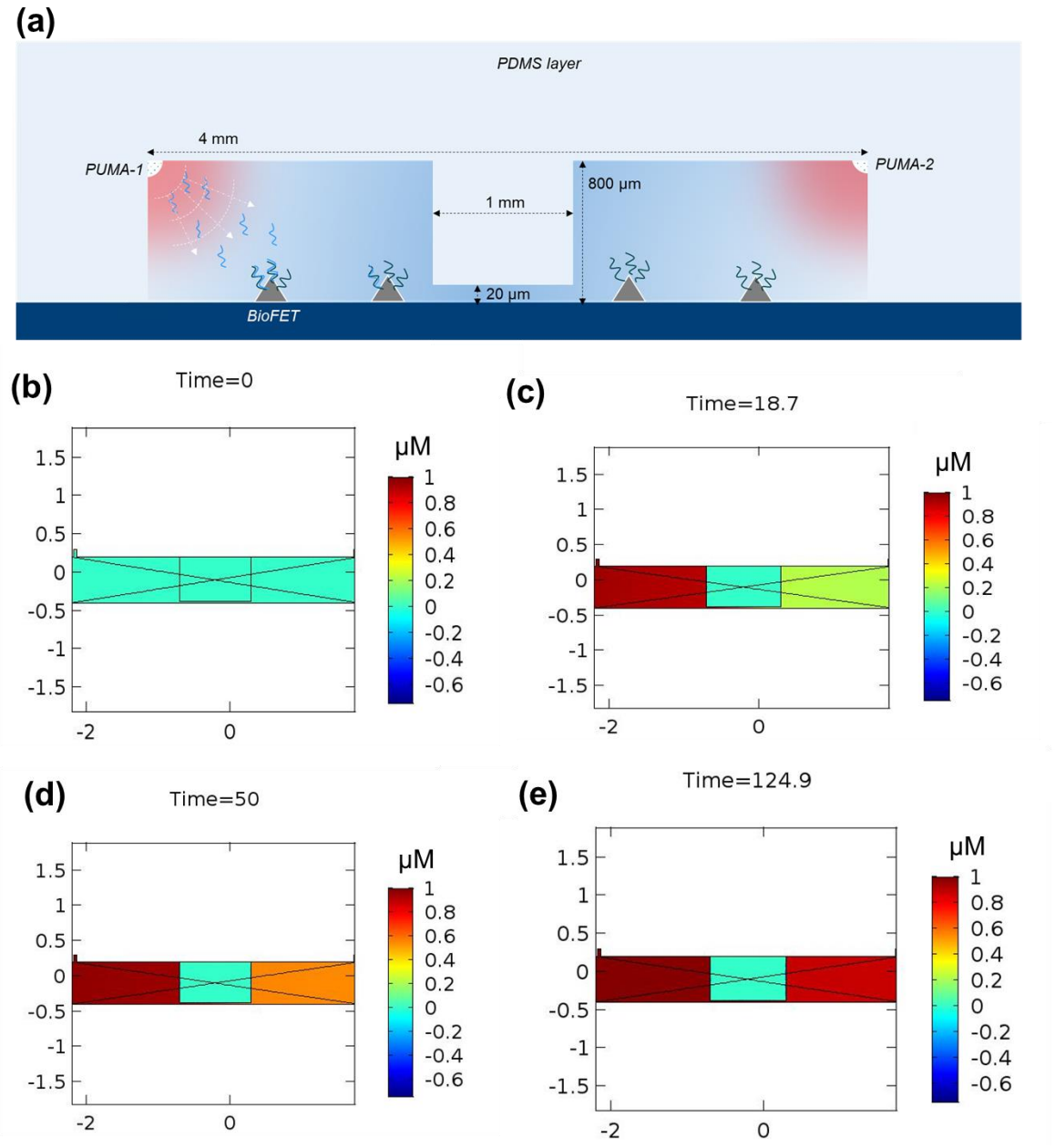

Figure 3: Reaction diffusion controlled mass transport of 12 bp DNAs while introducing a rectangular shape septum in the middle of the fluidic volume creating a capillary of 1 mm (length) × 20 µm (height) × 50 µm (width). (a) schematic illustration of the set-up, (b-d) DNA concentration due to reaction-diffusion mass transport after the start of PUMA-1 shown at 0, 18.7, 50 and 125 minutes.

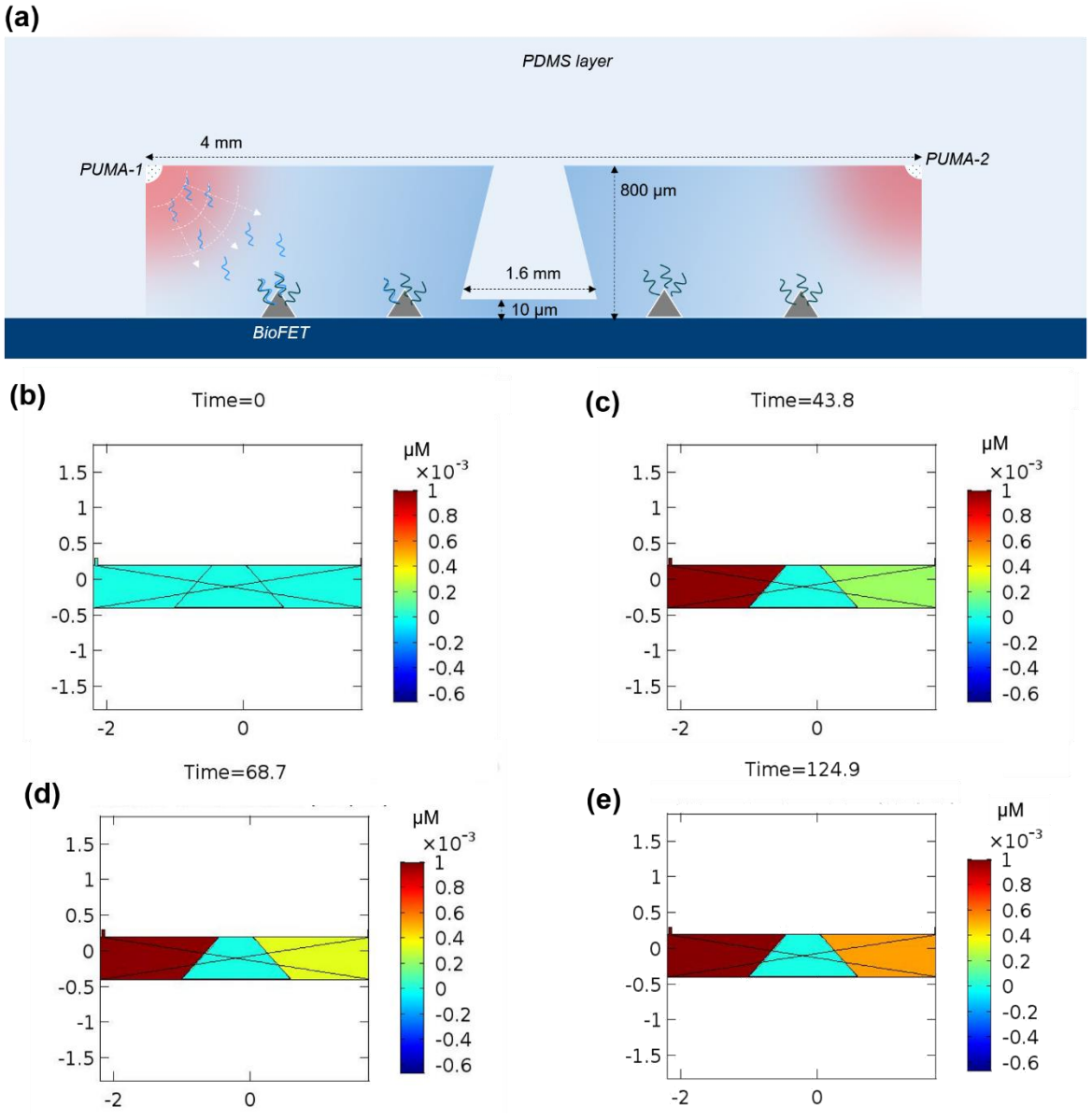

Figure 4: Reaction diffusion controlled mass transport of 12 bp DNAs while introducing a trapezoidal shape septum in the middle of the fluidic volume creating a capillary of 1.6 mm (length) × 10 µm (width) × 50 µm (height). (a) schematic illustration of the set-up, (b-d) DNA concentration due to reaction-diffusion mass transport after the start of PUMA-1 shown at 0, 18.7, 50 and 125 minutes, which is much slower than the set-up with rectangular septum.

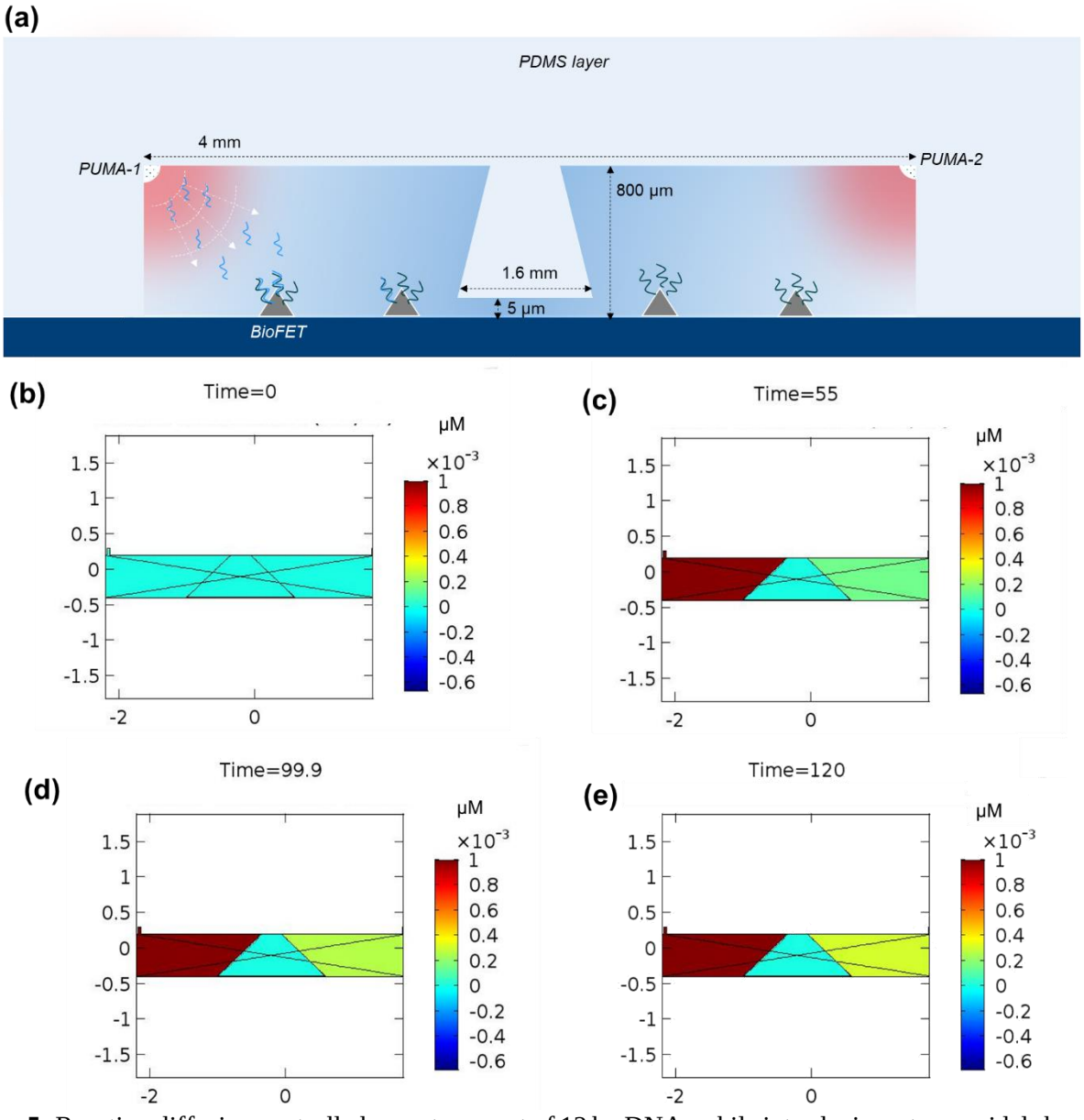

Figure 5: Reaction diffusion controlled mass transport of 12 bp DNAs while introducing a trapezoidal shape septum in the middle of the fluidic volume creating a capillary of 1.6 mm (length) × 10 µm (width) × 50 µm (height). (a) schematic illustration of the set-up, (b-d) DNA concentration due to reaction-diffusion mass transport after the start of PUMA-1 shown at 0, 55, 100 and 120 minutes, which is favourable for being slower than the previous two set-ups.

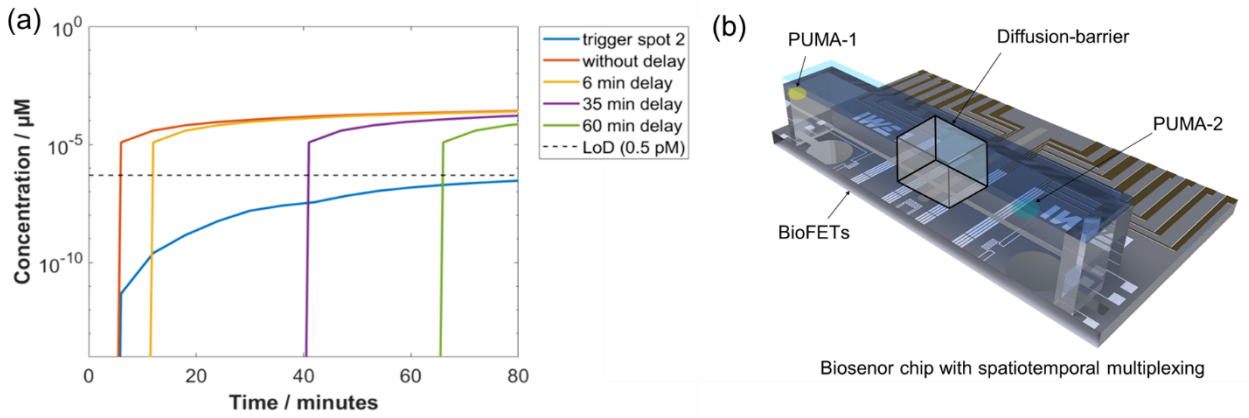

Figure 6: Reaction-diffusion regulated spatiotemporal multiplexing on chip. (a) The graph shows concentration of PUMA output DNA sequence at BioFET interface closer to the release spot 1 (b) Illustration of the biosensor chip with reaction-diffusion fluidic volume on top. The PUMA output DNA concentrations at different time intervals, exponential increase of concentration at the interface due to reaction-diffusion regulated mass transport and saturation is simulated. The blue curve shows the concentration evolution of output DNA sequence from release spot 2, which for the given time domain remain below the limit-of-detection of the BioFETs.

References:

1. T. M. Squires, andS. R. Quake, "Microfluidics: Fluid physics at the nanoliter scale," Rev Mod Phys **77**, 977 (2005).
2. S. Chen, andG. Seelig, "Programmable patterns in a DNA-based reaction-diffusion system," Soft Matter **16**, 3555 (2020).
3. J. H. Zhang, J. Q. Song, F. Z. Mou, J. G. Guan, andA. Sen, "Titania-Based Micro/Nanomotors: Design Principles, Biomimetic Collective Behavior, and Applications," Trends Chem **3**, 387 (2021).
4. L. F. Marcos, S. L. Wilson, andP. Roach, "Tissue engineering of the retina: from organoids to microfluidic chips," J Tissue Eng **12**, 20417314211059876 (2021).
5. J. Yu, E. Berthier, A. Craig, T. E. de Groot, S. Sparks, P. N. Ingram, D. F. Jarrard, W. Huang, D. J. Beebe, andA. B. Theberge, "Reconfigurable open microfluidics for studying the spatiotemporal dynamics of paracrine signalling," Nat Biomed Eng **3**, 830 (2019).
6. C. Tian, Q. Tu, W. Liu, andJ. Wang, "Recent advances in microfluidic technologies for organ-on-a-chip," Trac-Trend Anal Chem **117**, 146 (2019).
7. K. Ishida, andT. Mitsui, "Role of the boundary in feather bud formation on one-dimensional bioengineered skin," APL Bioeng **2**, 016107 (2018).
8. M. H. Elsafi Mabrouk, R. Goetzke, G. Abagnale, B. Yesilyurt, L. Salz, O. Cypris, P. Gluck, S. Liesenfelder, K. Zeevaert, Z. Ma, M. A. S. Toledo, R. Li, I. G. Costa, A. Lampert, V. Pachauri, U. Schnakenberg, M. Zenke, andW. Wagner, "The spatial self-organization within pluripotent stem cell colonies is continued in detaching aggregates," Biomaterials **282**, 121389 (2022).
9. K. F. Sonnen, andC. A. Merten, "Microfluidics as an Emerging Precision Tool in Developmental Biology," Dev Cell **48**, 293 (2019).
10. B. Lu, Y. C. Zhou, G. A. Huber, S. D. Bond, M. J. Holst, andJ. A. McCammon, "Electrodiffusion: a continuum modeling framework for biomolecular systems with realistic spatiotemporal resolution," J Chem Phys **127**, 135102 (2007).
11. S. Lin, Y. Liu, M. Zhang, X. Xu, Y. Chen, H. Zhang, andC. Yang, "Microfluidic single-cell transcriptomics: moving towards multimodal and spatiotemporal omics," Lab Chip **21**, 3829 (2021).
12. M. Javanainen, H. Martinez-Seara, C. V. Kelly, P. Jungwirth, andB. Fabian, "Anisotropic diffusion of membrane proteins at experimental timescales," J Chem Phys **155**, 015102 (2021).
13. K. H. Stern, "The Liesegang Phenomenon," Chemical Reviews **54**, 79 (1954).
14. A. N. Zaikin, andA. M. Zhabotinsky, "Concentration wave propagation in two-dimensional liquid-phase self-oscillating system," Nature **225**, 535 (1970).
15. A. T. Winfree, "Scroll-shaped waves of chemical activity in three dimensions," Science **181**, 937 (1973).
16. J. Ross, S. C. Muller, andC. Vidal, "Chemical waves," Science **240**, 460 (1988).
17. S. Jakubith, H. H. Rotermund, W. Engel, A. von Oertzen, andG. Ertl, "Spatiotemporal concentration patterns in a surface reaction: Propagating and standing waves, rotating spirals, and turbulence," Physical review letters **65**, 3013 (1990).
18. S. C. Muller, "Geometric and Dynamic Properties of Chemical Waves," React Kinet Catal L **42**, 289 (1990).
19. A. T. Winfree, "The Prehistory of the Belousov-Zhabotinsky Oscillator," J Chem Educ **61**, 661 (1984).
20. S. Deshpande, F. Brandenburg, A. Lau, M. G. F. Last, W. K. Spoelstra, L. Reese, S. Wunnava, M. Dogterom, andC. Dekker, "Spatiotemporal control of coacervate formation within liposomes," Nat Commun **10**, 1800 (2019).
21. N. Shanks, "Modeling Biological Systems: The Belousov–Zhabotinsky Reaction," Foundations of Chemistry **3**, 33 (2001).
22. G. Ashkenasy, T. M. Hermans, S. Otto, andA. F. Taylor, "Systems chemistry," Chem Soc Rev **46**, 2543 (2017).

23. C. Floyd, G. A. Papoian, andC. Jarzynski, "Gibbs free energy change of a discrete chemical reaction event," J Chem Phys **152**, 084116 (2020).
24. T. Prustel, andM. Meier-Schellersheim, "Space-time histories approach to fast stochastic simulation of bimolecular reactions," J Chem Phys **154**, 164111 (2021).
25. J. Pantoja-Hernandez, V. F. Brena-Medina, andM. Santillan, "Hybrid reaction-diffusion and clock-and-wavefront model for the arrest of oscillations in the somitogenesis segmentation clock," Chaos **31**, 063107 (2021).
26. A. Laskar, O. E. Shklyaev, andA. C. Balazs, "Controlling the Spatiotemporal Transport of Particles in Fluid-Filled Microchambers," Langmuir **36**, 7124 (2020).
27. N. Hao, P. Liu, H. Bachman, Z. Pei, P. Zhang, J. Rufo, Z. Wang, S. Zhao, andT. J. Huang, "Acoustofluidics-Assisted Engineering of Multifunctional Three-Dimensional Zinc Oxide Nanoarrays," ACS Nano **14**, 6150 (2020).
28. D. Chatterjee, andB. J. Cherayil, "Anomalous reaction-diffusion as a model of nonexponential DNA escape kinetics," J Chem Phys **132**, 025103 (2010).
29. I. Pereiro, A. Fomitcheva-Khartchenko, andG. V. Kaigala, "Shake It or Shrink It: Mass Transport and Kinetics in Surface Bioassays Using Agitation and Microfluidics," Anal Chem **92**, 10187 (2020).
30. D. Rani, Y. Singh, M. Salker, X. T. Vu, S. Ingebrandt, andV. Pachauri, "Point-of-care-ready nanoscale ISFET arrays for sub-picomolar detection of cytokines in cell cultures," Anal Bioanal Chem **412**, 6777 (2020).
31. A. Erbas, M. Olvera de la Cruz, andJ. F. Marko, "Receptor-Ligand Rebinding Kinetics in Confinement," Biophys J **116**, 1609 (2019).
32. L. E. Delle, V. Pachauri, A. Vlandas, M. Riedel, B. Lägel, R. Lilischkis, X. T. Vu, P. Wagner, R. Thoelen, F. Lisdat, andS. Ingebrandt, "Scalable fabrication and application of nanoscale IDE-arrays as multi-electrode platform for label-free biosensing," Sensors and Actuators B: Chemical **265**, 115 (2018).
33. H. Parsa, C. D. Chin, P. Mongkolwisetwara, B. W. Lee, J. J. Wang, andS. K. Sia, "Effect of volume- and time-based constraints on capture of analytes in microfluidic heterogeneous immunoassays," Lab Chip **8**, 2062 (2008).
34. G. Figueroa-Miranda, Y. Liang, M. Suranglikar, M. Stadler, N. Samane, M. Tintelott, Y. Lo, J. A. Tanner, X. T. Vu, J. Knoch, S. Ingebrandt, A. Offenhausser, V. Pachauri, andD. Mayer, "Delineating charge and capacitance transduction in system-integrated graphene-based BioFETs used as aptasensors for malaria detection," Biosens Bioelectron **208**, 114219 (2022).
35. T. Jet, G. Gines, Y. Rondelez, andV. J. C. S. R. Taly, "Advances in multiplexed techniques for the detection and quantification of microRNAs," **50**, 4141 (2021).
36. Y. Rondelez, andG. Gines, "Multiplex Digital MicroRNA Detection Using Cross-Inhibitory DNA Circuits," ACS Sens **5**, 2430 (2020).
37. G. Gines, R. Menezes, K. Nara, A. S. Kirstetter, V. Taly, andY. Rondelez, "Isothermal digital detection of microRNAs using background-free molecular circuit," Sci Adv **6**, eaay5952 (2020).
38. M. Tintelott, V. Pachauri, S. Ingebrandt, andX. T. Vu, "Process variability in top-down fabrication of silicon nanowire-based biosensor arrays," Sensors **21**, 5153 (2021).
39. J. Rodriguez-Manzano, K. Malpartida-Cardenas, N. Moser, I. Pennisi, M. Cavuto, L. Miglietta, A. Moniri, R. Penn, G. Satta, andP. J. A. c. s. Randell, "Handheld point-of-care system for rapid detection of SARS-CoV-2 extracted RNA in under 20 min," **7**, 307 (2021).
40. C. Toumazou, L. M. Shepherd, S. C. Reed, G. I. Chen, A. Patel, D. M. Garner, C.-J. A. Wang, C.-P. Ou, K. Amin-Desai, andP. J. N. m. Athanasiou, "Simultaneous DNA amplification and detection using a pH-sensing semiconductor system," **10**, 641 (2013).
41. E. Chirshev, K. C. Oberg, Y. J. Ioffe, J. J. J. C. Unternaehrer, andt. medicine, "Let-7 as biomarker, prognostic indicator, and therapy for precision medicine in cancer," **8**, 1 (2019).

42. M. Tintelott, T. Kremers, S. Ingebrandt, V. Pachauri, andX. T. Vu, "Realization of a PEDOT: PSS/Graphene Oxide On-Chip Pseudo-Reference Electrode for Integrated ISFETs," Sensors **22**, 2999 (2022).
43. M. Tintelott, S. Ingebrandt, V. Pachauri, andX. T. Vu, *Lab-on-a-chip based silicon nanowire sensor system for the precise study of chemical reaction-diffusion networks* (VDE, 2021).
44. A. S. Zadorin, Y. Rondelez, J.-C. Galas, andA. Estevez-Torres, "Synthesis of programmable reaction-diffusion fronts using DNA catalyzers," Physical review letters **114**, 068301 (2015).
45. I. Kurylo, G. Gines, Y. Rondelez, Y. Coffinier, andA. Vlandas, "Spatiotemporal control of DNA-based chemical reaction network via electrochemical activation in microfluidics," Sci Rep **8**, 6396 (2018).
46. A. Baccouche, K. Montagne, A. Padirac, T. Fujii, andY. Rondelez, "Dynamic DNA-toolbox reaction circuits: a walkthrough," Methods **67**, 234 (2014).
47. M. El-Hachem, S. W. McCue, W. Jin, Y. Du, andM. J. Simpson, "Revisiting the Fisher-Kolmogorov-Petrovsky-Piskunov equation to interpret the spreading-extinction dichotomy," Proc Math Phys Eng Sci **475**, 20190378 (2019).
48. M. Gries, A. Christmann, S. Schulte, M. Weyland, S. Rommel, M. Martin, M. Baller, R. Roth, S. Schmitteckert, M. Unger, Y. Liu, F. Sommer, T. Muhlhaus, M. Schroda, J. P. Timmermans, I. Pintelon, G. A. Rappold, M. Britschgi, H. Lashuel, M. D. Menger, M. W. Laschke, B. Niesler, andK. H. Schafer, "Parkinson mice show functional and molecular changes in the gut long before motoric disease onset," Mol Neurodegener **16**, 34 (2021).
49. D. Mangelinck, T. Luo, andC. Girardeaux, "Reactive diffusion in the presence of a diffusion barrier: Experiment and model," J Appl Phys **123**, 185301 (2018).
50. P. Nair, andM. Alam, "Performance limits of nanobiosensors," Applied physics letters **88**, 233120 (2006).